ESR centers in reduced stabilized zirconia

R. Ben-Michael, D. S. Tannhauser, and J. Genossar
Department of Physics, Technion, Israel Institute of Technology, Haifa, Israel
(Received 15 January 1990; revised manuscript received 9 August 1990)

Stabilized zirconia, when exposed at high temperature to a reducing atmosphere, becomes colored, and a pronounced room-temperature ESR signal appears. The concentration of the color centers was determined by optical absorption in the uv–visible range, and the concentration of the paramagnetic centers was determined by electron paramagnetic resonance in the X band. We found that the concentrations of the centers causing the two effects have the same $P(O_2)^{-1/4}$ dependence on the oxygen pressure, a dependence that agrees with a simple model; however, the ESR signal varies strongly from crystal to crystal. We conclude from these results that both effects are caused by the same center, most probably an impurity with a total concentration of 10^{-3} mol, which has captured an electron. From the ESR results the level of this electron state is $\simeq 1.60$ eV below the conduction band. The oscillator strength for optical absorption was found to be $f_O \cong 0.01$.

I. INTRODUCTION

We have recently published a preliminary analysis of experimental results concerning quantitative ESR measurements on reduced yttria-stabilized zirconia (YSZ).[1] In common with Thorp *et al.*[2] we interpreted the signal as originating from singly ionized oxygen vacancies bound to a Y ion. A similar interpretation based on O^- ion was published by Ermakovich *et al.*[3] In the present article we reanalyze our previous and new ESR and also optical absorption experimental results and conclude that the ESR center in stabilized zirconia is most probably an impurity with a concentration of about 0.1 mol. %. We reported this revised conclusion briefly before.[4]

At high temperature, zirconia (ZrO_2) has the cubic CaF_2 structure. This structure is not stable at room temperature, but can be stabilized by addition of about 10 mol % Y_2O_3 (or some other oxides such as CaO or MgO). If the mol fraction of Y_2O_3 is y we have $Zr_{1-x}Y_xO_{2-x/2}$ with $x=2y/(1+y)$. The mol fraction of vacancies in the oxygen sublattice is therfore $x/4$, these vacancies have an effective charge of 2+ and are compensated by the Y ions with their effective charge of 1−.

The above composition will be called the stoichiometric one. In practice the sample is never exactly stoichiometric, and the extra or missing oxygen ions are balanced by charge defects, namely, vacancies or impurities which have trapped an electron and by free electrons and holes (see below). Samples annealed in a strongly reducing atmosphere contain free electrons while samples annealed in a weakly reducing or oxydizing atmosphere contain free holes.[5] Weppner[6] has used his results of conductance and diffusion measurements to determine the concentration of free electrons and holes in $Zr_{0.82}Y_{0.18}O_{1.91}$ (10 mol % Y_2O_3) in the temperature range 700–900 °C. Single crystals of stabilized zirconia which have been exposed to a reducing atmosphere become colored, and a pronounced ESR signal appears. We shall show in the present paper that the origin of the ESR signal is an impurity center which has captured an electron in an energy level 1.6 eV below the conduction band.

The observed coloration is caused by two types of color centers[7] with maximum absorption at 365 nm (yellow color of the crystal) and at 480 nm (dark brown color). We reported[8] on the reoxidation kinetics of the dark brown centers before. The yellow color centers appear together with the paramagnetic centers, whereas the dark brown centers are not ESR active. In this paper we show that the same defect gives rise both to the ESR signal and the yellow coloration.

II. EXPERIMENTAL PROCEDURE

Our measurements were taken on samples cut from five zirconia crystals stabilized with Y_2O_3 and one crystal stabilized with CaO. The nominal compositions are given in Table I. Possible uncontrolled impurities are, according to the manufactures Ti, Fe, and Si in samples S–SH and Co in sample SE. HfO_2 is brought in with the starting material.

Our standard sample size for ESR was $6\times2\times2$ mm^3 with the long edge in the [110] direction and the two short edges in the [$\bar{1}$10] and [001] directions. For the optical absorption measurements, we cut a sample with dimensions $2\times7\times7$ mm^3 from crystal SH.

The samples were annealed at various temperatures in the range 700–1050 °C in flowing H_2-H_2O mixtures and cooled quickly by pushing the boat holding them out of the hot zone. We estimate the initial cooling rate to be about 30 °C/sec. For the comparison of ESR and color center densities, the two samples to be measured were annealed simultaneously. The oxygen pressure was calculated using standard tables and checked with a $P(O_2)$ meter based on stabilized zirconia (Thermox Instruments). This treatment removes oxygen from the sample and produces, as mentioned, both yellow color and paramagnetism. Some anneals were done in flowing hydrogen, in this case $P(O_2)$ was read from the oxygen meter. Some samples were wrapped in zirconium foil during the annealing in pure hydrogen, or annealed in a closed quartz

TABLE I. Concentration of the constituent in zirconia crystals in mol % (manufacturers information).

	Sample	ZrO_2	HfO_2	Y_2O_3	CaO	CeO_2	Nd_2O_3	CoO
1	S	89.5	1.0	9.4		0.1		
2	SA	84.0	1.0	15.0				
3	SC	87.0	1.0	12.0				
4	SD	89.5	1.0	9.4		0.05	0.006	
5	SE	84?	1.0		15?			traces
6	SH	89.5	1.0	9.4				

capsule with zirconium metal present. This gave a deeper reduction, but $P(O_2)$ was then not well defined, we estimate $P(O_2) \leq 10^{-30}$ atm. (The equilibrium pressure of oxygen over metallic Zr is 10^{-39} atm at 900 °C.)

In the spectrophotometer (Beckman ACTA M VII) we measured the optical transmission in the range 250–700 nm. The transmission spectrum of the oxidized colorless sample served as a baseline for determination of absorption by the colored crystals. It was recorded in a disk file, using a personal computer which serves as a data acquisition system. The spectrophotometer was not quite consistent in its zero transmission line. We corrected this by adding (sometimes subtracting) up to 5% to the transmission, until its value at 700 nm, well outside the absorption range of the color centers, was equal to that of the transparent sample.

III. EXPERIMENTAL RESULTS

A. ESR line shape and symmetry

In all reduced samples a pronounced line appears which consists of up to four components. In Fig. 1 we show ESR lines recorded under various conditions. The separate components are visible when the sample is oriented in a random direction with respect to the magnetic field. We determined previously[9] that the ESR center responsible for this line has axial symmetry with a ⟨111⟩ direction as symmetry axis, where $g_{\parallel} = 1.989$ and $g_{\perp} = 1.860$. When the magnetic field is parallel to one of the [100] directions all four components coalesce into one line at $g = 1.905$, except for a small satellite at $g = 2.008$ [Fig. 1(b)]. The shape of this line was the same for all samples. The same line also appears on irradiation of samples with x rays, thus proving that it is not caused by hydrogen entering the sample. An x ray induced line bleaches in a few days at room temperature.

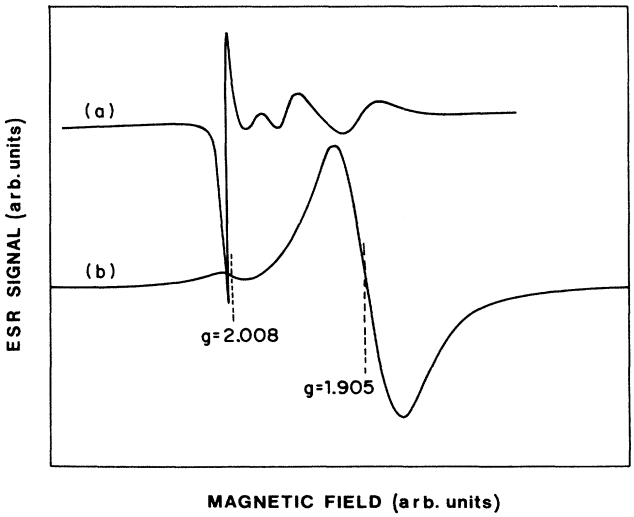

FIG. 1. ESR derivative signal in reduced zirconia when the magnetic field is (a) in a random direction (measurement at 100 K), and (b) parallel to [100] (measurement at room temperature).

B. Quantitative ESR results

Quantitative measurements of the ESR center concentration were done with the magnetic field parallel to the [100] direction and the sample at room temperature. As the line width was approximately the same in all samples and was also independent of signal strength, the peak-to-peak height of the derivative signal divided by the sample weight was taken as a measure of the spin concentration, $[C_{ESR}]$.

We show in Fig. 2 isotherms of $[C_{ESR}]$ at 970 °C for a number of samples quenched from various temperatures in the range 900–1050 °C. Results showed that a quenching temperature of $T > 970$ °C was equivalent to 970 °C, the equilibration with the atmosphere proceeding faster than the cooling in this range. Only a few of the measurements were taken at $T < 970$ °C, these were normalized to 970 °C using the temperature dependence of Fig. 3. For all samples $[C_{ESR}]$ varies monotonically with the gas ratio $r = P(H_2O)/P(H_2)$ over the range of controlled or measured oxygen pressures. For crystals SA, SC, SD, and SH $\log_{10}[C_{ESR}]$ versus $\log_{10}P(O_2)$ is approximately linear with a slope of $-1/2$ [i.e., $[C_{ESR}]$ varies as $P(O_2)^{-1/4}$] while for crystals S and SE a steeper slope is seen. A dropoff is seen at the high pressure end of the measurements, except for crystal SH, while at the very low pressures obtained by annealing in the presence of zirconium, the signal seems to saturate. The slight residual increase in $[C_{ESR}]$ was not comparable to the very strong increase of the intensity of coloration (see below). Similar isotherms were obtained at 700 and 800 °C. Given the same annealing conditions and samples cut from the same crystal, $[C_{ESR}]$ was reproducible to ±10%, (e.g., the points given for crystal SA were taken on four different samples cut from the same boule) but differed widely from crystal to crystal.

Figure 3 shows the temperature dependence of $[C_{ESR}]$ at constant gas ratio ($\log_{10} r = -2$) for three samples. In spite of the large difference in absolute values, the slope of the three lines is the same.

C. Optical properties

All samples were colorless as received and could always be returned to this condition by annealing in air at 950 °C for a few minutes. Samples annealed in reduced

$P(O_2)$ were more or less strongly colored. Those annealed in H_2 (with and without water) turned yellow except for the samples containing Ce (S and SD) which acquired a pronounced orange color. In all samples the intensity of coloration increased with decrease of $P(O_2)$. Quantitative measurements were done on a sample cut from crystal SH.

In Fig. 4 we show a typical transmission spectrum of sample SH that had been reduced in an H_2-H_2O atmosphere, and the transmission of the same sample when colorless. The center of the absorption line is at 400 nm while the absorption edge of the transparent sample is at 325 nm which corresponds to a band gap of $E_{gap}=3.81$ eV.

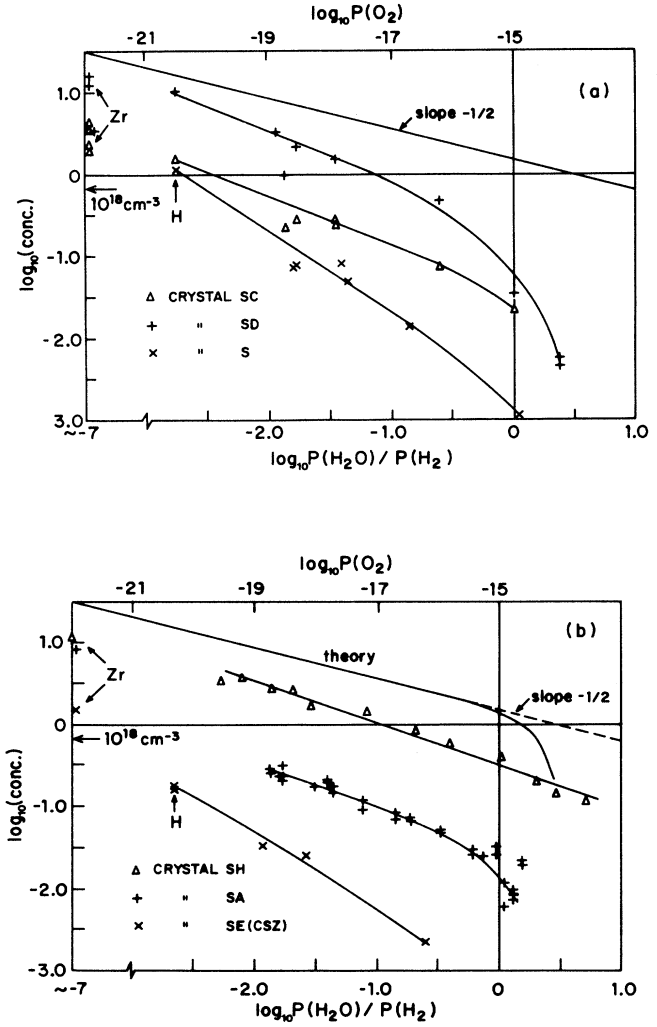

FIG. 2. (a) Relative spin concentration in six zirconia crystals quenched from $T>=900$°C vs. gas ratio during annealing. The effective quenching temperature is 970°C, see text. For the points marked H, the gas ratio was calculated from the oxygen pressure measured in H_2. The points marked Zr refer to samples wrapped in zirconium foil. The lines are drawn to guide the eye. The theoretical spin concentration behavior in the presence of a compensating impurity is shown in (b). The oxygen pressures at 970°C corresponding to the gas ratios are indicated along the top edge.

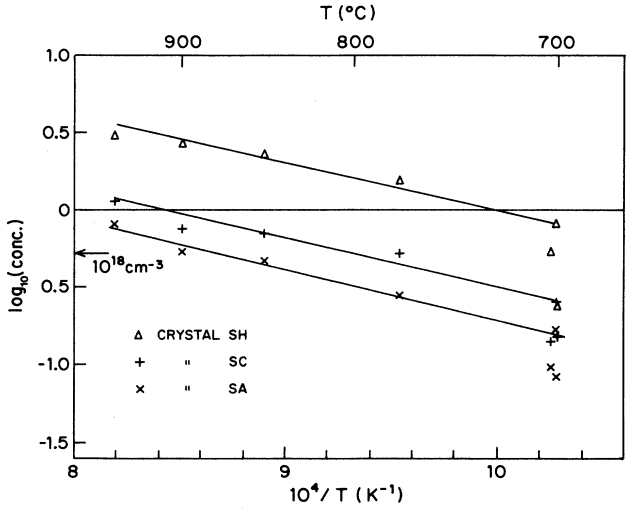

FIG. 3. Dependence of $[C_{ESR}]$ on quenching temperature for crystals SA, SC, SH at $\log_{10}r=-2$.

Samples which were annealed in the presence of zirconium foil turned very dark brown, almost opaque. In Fig. 5 we show transmission spectra of a sample when transparent (oxidized), after it had been annealed in flowing hydrogen and after annealing in a closed quartz capsule together with metallic zirconium. The oxygen pressure during the two reductions is estimated as 10^{-25} and 10^{-30} atm, respectively. These annealing conditions produce in addition to the yellow centers also dark brown ones,[2,10] which shift the absorption edge towards the red. Measurements show[7] that the absorption line center for these brown samples is at 470 nm versus 365 nm for the yellow samples, i.e., on strong reduction a second kind of absorption center seems to appear.

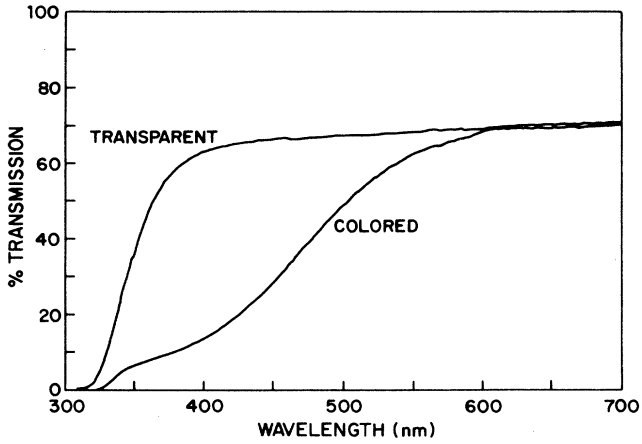

FIG. 4. Optical transmission of sample SH (9.5 mol % Y_2O_3) when transparent and after annealing at $\log_{10}P(H_2O)/P(H_2)=-1.70$.

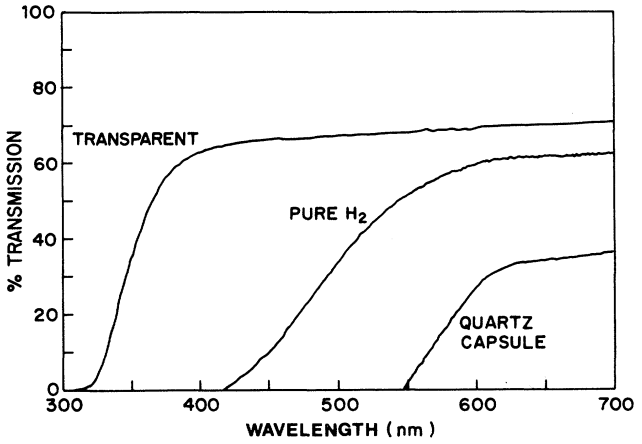

FIG. 5. Optical transmission as function of reduction during the annealing.

In Table II we compare three crystals which had been annealed in pure H_2 at 950 °C. We see that a stronger coloration goes together with a larger $[C_{\mathrm{ESR}}]$, and also with a shift of the absorption edge towards the red. This redshift is in contrast to PaiVerneker *et al.*[11] who reported a blueshift on strong reduction.

IV. DISCUSSION

We shall now explain the oxygen pressure dependence of $[C_{\mathrm{ESR}}]$ and show that the same centers are responsible for the ESR signal and the yellow color. We shall argue that these centers are impurities which have trapped an electron.

A. Oxygen pressure dependence

As previously noted[9] we can deduce from the orientation dependence of the main ESR line that the center giving rise to it has axial symmetry, with a ⟨111⟩ direction as symmetry axis. We shall now show that the ESR active center can be either a vacancy or an impurity, for both cases we get the same dependence of $[C_{\mathrm{ESR}}]$ proportional to $P(\mathrm{O}_2)^{-1/4}$, as observed.

We follow the Kroeger-Vink notation, concentrations, [ ], are in cm^{-3}. To describe the high-temperature equilibrium of YSZ with a given $P(\mathrm{O}_2)$ we consider the following defect-related reactions

$$\mathrm{O_O} \leftrightarrow \tfrac{1}{2}\mathrm{O}_2(\mathrm{gas}) + V_{\mathrm{O}}^{x} \,, \tag{1}$$

$$V_{\mathrm{O}}^{x} \leftrightarrow V_{\mathrm{O}}^{\cdot} + e \,, \tag{2}$$

$$V_{\mathrm{O}}^{\cdot} \leftrightarrow V_{\mathrm{O}}^{\cdot\cdot} + e \,, \tag{3}$$

$$\mathrm{F}^{m'} \leftrightarrow \mathrm{F}^{(m-1)'} + e \,, \tag{4}$$

which describe the creation of a neutral vacancy and excitation of an electron from a neutral or singly ionized vacancy or an impurity to the conduction band. Here we assume that the impurity F can be in two states, with m and with $m-1$ effective negative charges, where m can also be zero or negative. Introduction of more than one impurity into these equation would not change the conclusions and is therefore not done.

The following chemical equilibrium relations hold

$$[V_{\mathrm{O}}^{x}] = K_x(T) P(\mathrm{O}_2)^{-1/2} \,, \tag{5}$$

$$[V_{\mathrm{O}}^{\cdot}] n = K_1(T)[V_{\mathrm{O}}^{x}] \,, \tag{6}$$

$$[V_{\mathrm{O}}^{\cdot\cdot}] n = K_2(T)[V_{\mathrm{O}}^{\cdot}] \,, \tag{7}$$

$$[\mathrm{F}^{(m-1)'}] n = K_3(T)[\mathrm{F}^{m'}] \,. \tag{8}$$

We also have intrinsic excitation

$$np = K_i(T) \,, \tag{9}$$

conservation of the number of impurities

$$[\mathrm{F}^{(m-1)'}] + [\mathrm{F}m'] = [\mathrm{F}^{\mathrm{tot}}] \,, \tag{10}$$

and finally the neutrality condition

$$p + [V_{\mathrm{O}}^{\cdot}] + 2[V_{\mathrm{O}}^{\cdot\cdot}] = n + [Y'_{\mathrm{Zr}}] + m[\mathrm{F}^{m'}] + (m-1)[\mathrm{F}^{(m-1)'}] \,. \tag{11}$$

[Equation (11) is valid for YSZ. A similar equation holds for CSZ, calcia stabilized zirconia.]

In these equations $K_x = f(T)\exp(-\Delta\mu_{xO}/kT)$, $K_i = N_C N_V \exp(-E_g/kT)$, $K_1 = N_C \exp(-E_1/kT)$, $K_2 = N_C \exp(-E_2/kT)$, and $K_3 = N_C \exp(-E_3/kT)$ where E_g is the bandgap, $\Delta\mu_{xO}, E_1, E_2$, and E_3 are the enthalpy changes in reactions (1) to (4) and N_C and N_V are the effective number of states in the conduction and valence bands, respectively.

If we write the formula of the material as $\mathrm{Zr}_{1-x}\mathrm{Y}_u\mathrm{F}_v^{m'}\mathrm{F}_w^{(m-1)'}\mathrm{O}_{2-\epsilon-u/2}$ (where we assume that all cation sites are occupied, i.e., $u+v+w=x$) it can be shown that ϵ, the deviation from stoichiometry, is given by

TABLE II. Absorption edge and concentration of paramagnetic and color centers for different crystals annealed in pure H_2 at 950 °C.

	Crystal	Absorption edge (nm)	Band gap (eV)	Concentration of Color centers	Concentration of ESR centers
SF	15 mol % CaO	295	4.20	Low	Low
SG	15 mol % Y_2O_3	300	4.13	Medium	Medium
SH	9.5 mol % Y_2O_3	325	3.81	High	High

$$\epsilon=\tfrac{1}{2}\{[Y'_{Zr}]-2[V_O^{tot}]\}$$
$$=\tfrac{1}{2}\{n-p+m[F^{m'}]+(m-1)[F^{(m-1)'}]$$
$$+[V_O^{\cdot}]+2[V_O^x]\} \quad (12)$$

(all concentrations pertain to high temperature).

Since the dominant vacancy species in stabilized zirconia is always the doubly ionized oxygen vacancy $V_O^{\cdot\cdot}$ and changes in composition are small, we have to a very good approximation $2[V_O^{\cdot\cdot}]=[Y'_{Zr}]$. We then get from Eqs. (5)–(7) that

$$n=\left[\frac{2K_1K_2K_x}{[Y'_{Zr}]}\right]^{1/2}P(O_2)^{-1/4} \quad (13)$$

and it follows from (9) that p is proportional to $P(O_2)^{1/4}$. The oxygen pressure dependence of n and p in Weppner's[6] Fig. 5 is based on these relations. Equation (7) gives now that

$$[V_O^{\cdot}]=\left[\frac{[Y'_{Zr}]K_1K_x}{2K_2}\right]^{1/2}P(O_2)^{-1/4}, \quad (14)$$

and it follows similarly from Eq. (8) that for an impurity for which $[F^{m'}]\ll[F^{tot}]$,

$$[F^{m'}]=\frac{F^{tot}}{K_3}\left[\frac{2K_1K_2K_x}{[Y'_{Zr}]}\right]^{1/2}P(O_2)^{-1/4}, \quad (15)$$

i.e., at high temperatures n, $[V_O^{\cdot}]$ and $[F^{m'}]$ all have the same dependence on $P(O_2)$.

When the sample is cooled quickly to room temperature (which we shall take as effectively 0 K) the stoichiometry does not change, but all electrons fall to the lowest available level. In order to simplify the discussion we shall treat separately the cases that the ESR centers generated in this process are vacancies and that they are impurities.

If the ESR centers are vacancies, then they have to be $V_O^{\cdot}$ centers as V_O^x contains two electrons. Since a possible electronic reaction is

$$2V_O^{\cdot}\leftrightarrow V_O^x+V_O^{\cdot\cdot}+E_1-E_2 \quad (16)$$

we have to assume that $E_2>E_1$ to make this reaction proceed to the left on cooling. As we assumed that electrons are not captured by the impurities, we must also have $E_2>E_3$.

We now get

$$[C_{ESR}]=[V_O^{\cdot}]_{RT}=[V_O^{\cdot}]_{HT}+2[V_O^x]_{HT}+[F^{m'}]_{HT}$$
$$+n-p, \quad (17)$$

where n and p refer to the high-temperature concentrations, which are independent of impurities [Eq. (13)]. We note that $[C_{ESR}]$ is much larger than n and p given by Weppner for our annealing conditions, so that these can be neglected. For any reasonable impurity concentration $[F^{tot}]\ll[V_O^{\cdot\cdot}]$. Equations (7) and (8) together with $E_2>E_3$ give $[V_O^{\cdot}]_{HT}\gg[F^{m'}]_{HT}$ and Eq. (17) gives

$$[C_{ESR}]=[V_O^{\cdot}]_{HT}+2[V_O^x]_{HT}. \quad (18)$$

If now $[V_O^{\cdot}]_{HT}\gg[V_O^x]_{HT}$ then $[C_{ESR}]\propto P(O_2)^{-1/4}$, as observed.

Equation (18) together with Eqs. (5) and (14) implies that $[C_{ESR}]$ should be independent of minor impurities and in the YSZ crystals should depend only on the yttrium concentration, which varies by less than a factor of 2 from crystal to crystal. However as seen in Fig. 2, $[C_{ESR}]$ varies from sample to sample by more than a factor of 30. We conclude threat the ESR centers cannot be ionized vacancies and have therefore to consider the case that $E_3>E_1,E_2$, i.e., that the lowest level available to the electrons lies on an impurity.

We have in this case

$$[C_{ESR}]=[F^{m'}]_{RT}=[V_O^{\cdot}]_{HT}+2[V_O^x]_{HT}$$
$$+[F^{m'}]_{HT}+n-p. \quad (19)$$

We neglect again n and p and, since $[V_O^{\cdot}]_{HT}$ and $[V_O^x]_{HT}$ are independent of impurity concentration, the variation of $[C_{ESR}]$ from crystal to crystal together with Eq. (19) implies that $[V_O^{\cdot}]_{HT}+2[V_O^x]_{HT}\ll[F^{m'}]_{HT}$. It follows that

$$[C_{ESR}]=[F^{m'}]_{HT}, \quad (20)$$

and we see from (15) that as long as $[F^{m'}]_{HT}\ll[F^{tot}]$, $[C_{ESR}]$ is expected to be proportional to $P(O_2)^{-1/4}$, as observed, but can vary widely from crystal to crystal.

We conclude that an impurity rather than a singly ionized vacancy is responsible for the ESR signal. This conclusion is supported by the saturation of $[C_{ESR}]$ at 0.1 mol % or less (see below), since the concentration of singly ionized vacancies should saturate only at about 3 mol %. A further argument for an impurity is given in Sec. IV C.

This explanation assumes that a reduced impurity is a paramagnetic center. The axial symmetry could then be explained by assuming that this paramagnetic ion with its effective negative charge attracts a vacancy.

In order to understand the quenching process better, we constructed a computer model using the above equations with $m=1$. Fig. 6 shows the concentration of various defects at 900 °C, which is a typical annealing temperature, the constants used are given in the figure caption. Figure 7 shows the same concentrations after quenching to 20 °C. We have assumed that the quenching is instantaneous so that ϵ, the deviation from stoichiometry defined in Eq. (12), stays constant. We also assumed here that $E_1>E_2$, this makes reaction (16) go to the right as needed for the model of strongly reduced crystals mentioned in Sec. IV E below.

We see from Fig 7 that indeed $[F^{m'}]$ varies as $P(O_2)^{-1/4}$ in the range of our annealing atmospheres $[-2.5<\log_{10}r<0.5$, corresponding to $-22<\log_{10}P(O_2)<-15$ atm, at 900 °C], that there is a sudden decrease in $[F^{m'}]$ at higher oxygen pressures, as indeed observed, (this is caused in our computer model by the increasing number of holes which appear at high $P(O_2)$ and act as electron traps on quenching) and that $[F^{m'}]$ saturates at $\log_{10}P(O_2)\simeq-30$ atm, all of which corresponds to our experimental findings. It is also in-

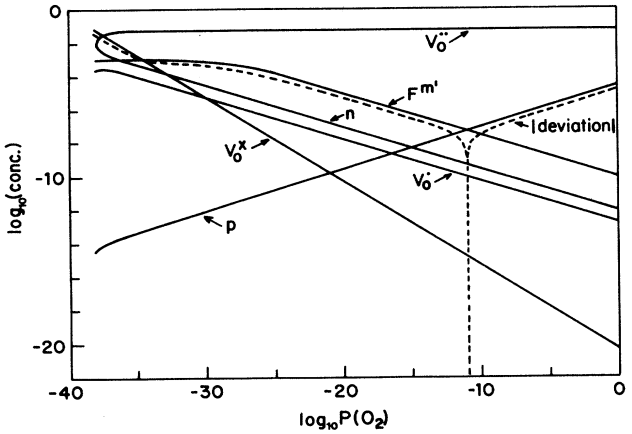

FIG. 6. Calculated concentration of defects in YSZ at 900 °C vs $P(O_2)$. The concentrations are per zirconium site (2.8×10^{22} sites/cm^3) and $P(O_2)$ is in atmospheres. The parameters used were $[Y_{Zr}]=0.119$, $\log_{10}n=-8.14$, $\log_{10}p=-8.4$, $\log_{10}[V_O^{\cdot}]=-9$ and $\log_{10}[V_O^x]=-12.6$ at 900 °C and $\log_{10}P(O_2)=-15$, $\log_{10}n=-11.4$ at 700 °C and same pressure, $E_g=3.9$ eV, $E_1=1.5$ eV, $E_2=1$ eV, and $E_3=1.6$ (the n,p, and E_g values are based on Ref. 6, Fig. 5, E_3 is based on the present paper, the values for $[V_O^{\cdot}]$, $[V_O^x]$, E_1 and E_2 are order of magnitude guesses). The absolute value of ϵ, the deviation from stoichiometry, is shown as a dotted line.

teresting to see that there is a sudden sharp decrease in V_O^x on going from $\log_{10}P(O_2)\simeq-32$ towards higher pressures, this might be connected with the fairly sharp color front which we have observed[8] on reoxidation and that at low pressure we get a high concentration of color centers. The concentrations of V_O^x and of $F^{m'}$ after quenching at low pressure are not very sensitive to the exact choice of E_1 and E_2 as long as $E_2<E_1<E_3$.

B. Correlation of color and $[C_{ESR}]$

In all crystals a correlation between $[C_{ESR}]$ and intensity of coloration was found. There is a saturation effect in $[C_{ESR}]$ which is not reflected in the coloration: very strong reduction, using Zr foil, increased $[C_{ESR}]$ only sightly, but increased the optical absorption very strongly. Also, as noted above, the optical absorption line of strongly reduced samples is not at the same wavelength as in samples reduced in controlled gas mixtures. We conclude that the center responsible for the deep coloration at very low $P(O_2)$ is not the ESR center. We shall argue below that the deep coloration is caused by V_O^x centers and that the number of such vacancies increases on quenching by reaction (16) proceeding to the right.

The area between the two transmission curves in Fig. 4 is a function of the concentration of the color centers. However it is more convenient to present the transmission data as absorption versus energy, using the following relations:

$$E\ (\text{eV})=1239.86/\lambda\ (\text{nm})\ ,$$

$$\mu(E)\ (\text{cm}^{-1})=\frac{1}{d}\ln\frac{T_S}{T_O}\ ,$$

where $\mu(E)$ is the absorption coefficient in cm^{-1} as a function of the energy, T_S the transmission of the colored sample, T_O the transmission of the same sample when transparent, and d the thickness of the sample, here 0.2 cm. A typical absorption spectrum is shown in Fig. 8. We see that the energy for maximum absorption is 3.4 ± 0.1 eV, i.e., at $\lambda=365\pm10$ nm (the error margin results from different data for different annealings of the same sample).

In Fig. 9 the area under the absorption curves for different anneals is plotted versus the gas pressure ratio during the annealing at 950 °C. We present also the area under the absorption curves before correction for apparatus error as detailed in Sec. II; it can be seen that this modification has indeed reduced the scatter of the points.

The concentration of the color centers was calculated

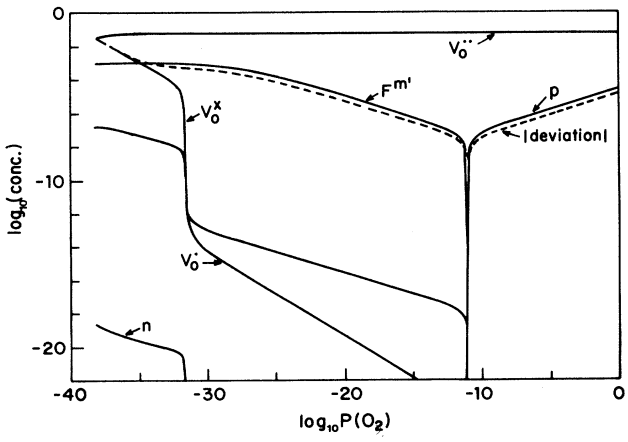

FIG. 7. Calculated concentration of defects in YSZ after quenching to room temperature from 900 °C. $P(O_2)$ is the equilibration pressure at 900 °C and the values given in the caption of Fig. 6 were used.

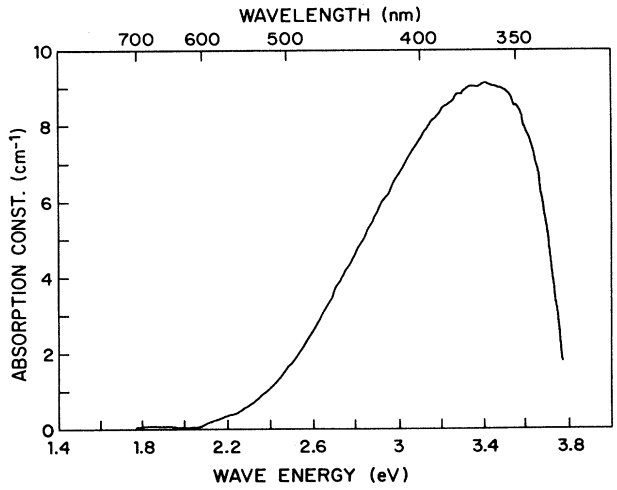

FIG. 8. Absorption of sample SH (9.5 mol % Y_2O_3) annealed at $\log_{10}P(H_2O)/P(H_2)=-1.70$. This curve was calculated from Fig. 4.

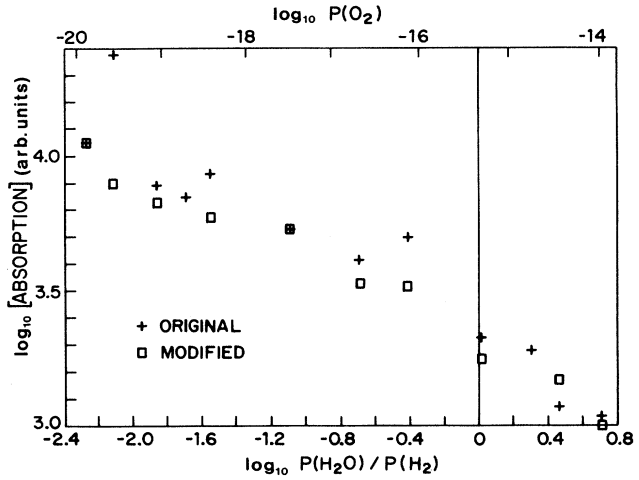

FIG. 9. Optical absorption of sample SH for different stages of coloration vs gas pressure ratio during annealing, taken from curves such as in Fig. 8. The oxygen pressure was calculated from the gas pressure ratio. The squares are modified points, see text.

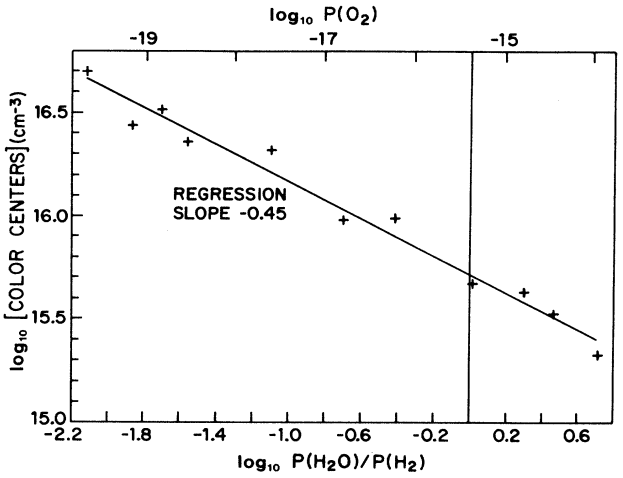

FIG. 10. Concentration of color centers vs gas pressure ratio at 950°C. The concentration was calculated using Eq. (21), and the area under curves such as Fig. 8.

using Dexter's modification of Smakula's equation[12]

$$N_O\ (\mathrm{cm}^{-3}) = 0.821\times 10^{17}\frac{n}{(n^2+2)^2 f_O}\int \mu(E)dE\ , \qquad (21)$$

where N_O is the concentration of color centers per cm^3, n is the index of refraction, for YSZ $n=2.2$, and f_O is the optical oscillator strength. For the integral we took the area under the absorption curves such as in Fig. 8.

In Fig. 10 the concentration of the color centers is plotted versus the gas pressure ratio during the anneals. For the oscillator strength we took initially $f_O=1$, this number is based on works done on alkali halides and on CaF_2 (Refs. 13 and 14) where f_O is of this order of magnitude. As we shall see below, this does not fit our results. The curve shown in Fig. 10 is a straight line with slope -0.45, which agrees with the slope of the graph for sample SH in Fig. 2(b) (-0.51), within the accuracy of our measurements. We therefore conclude that the color centers and the paramagnetic centers produced in stabilized zirconia when the material is annealed at $\log_{10}P(\mathrm{H_2O})/P(H_2) > -2.2$ (which corresponds at 950°C to $P(\mathrm{O_2}) > 10^{-20}$ atm) are the same.

We conclude that the relation between the observed concentrations is

$$\log_{10}(\text{ESR centers}) = K + \log(\text{color centers})\ . \qquad (22)$$

In Fig. 11 we plot $\log_{10}$(ESR centers) versus $\log_{10}$(color centers). We expect a linear dependence with a slope of $+1$. Indeed we get a straight line with slope $+0.84$. We believe that the difference between the slopes is due to the experimental errors.

The axes of Fig. 11 are marked in concentrations (cm^{-3}), assuming $f_O=1$. From Fig. 11 it is obvious that the oscillator strength is much smaller than 1. If we take $f_O=0.01$ in Eq. (4) we get similar values for the concentrations along both axes. Taking into account the uncertainties in the measurements we get for f_O, 0.005–0.02.

C. Concentration of impurity and location of its level

We can estimate the concentration of the impurity responsible for the ESR signal from the maximum strength of the signal for each crystal. We used $CuSO_4$ to calibrate our measurements in spins/cm^3, an absolute value is shown on the ordinate of Figs. 2(a) and 2(b), the uncertainty is estimated as a factor 2. The largest signal we measured, in crystal SD, which had been wrapped in Zr, corresponds to $[C_{\mathrm{ESR}}]=3\times 10^{19}\ \mathrm{cm}^{-3}$, i.e., 0.1 mol%. (There are 2.8×10^{22} metal ions/cm^3.) Because of the sat-

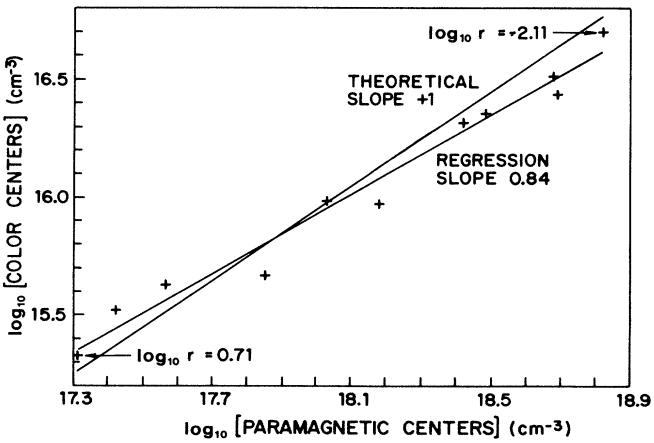

FIG. 11. Comparison between concentration of color and paramagnetic centers for different gas pressure ratios in the annealing process. Extreme pressure ratios, $r\equiv\log_{10}P(\mathrm{H_2O})/P(\mathrm{H_2})$, are indicated in the figure.

uration effect observed, this should be the actual impurity concentration in this crystal. This large value eliminates from consideration trace impurities and leaves just a few candidates which could give rise to the ESR signal. The actual element is at this moment unknown, analysis by proton induced x-ray emission (PIXE) showed no impurity whose concentration correlated with the strength of the signal. The large g shift ($\Delta g = g_e - g_{\parallel,\perp}$; where $g_e = 2.0023$ is the g value of a free electron), seems to argue for a multielectron ion. As the g value is less than that of a free electron, the impurity is presumably a paramagnetic one with a less-than-half-full shell. This eliminates, e.g., Cu, Fe, Co, and Ni but leaves Ti, V, Cr, Hf, Nb, Ta, W, etc. as possible candidates. The assumed impurity could be, for instance, titanium, which can exist as Ti^{3+} and as Ti^{4+}, the oxygen pressure and temperature controlling the ratio between the two valence states. This possibility is supported by the results of Ermakovich *et al.*[15] where an ESR line shape identical to ours was found for Ti doped samples. ENDOR measurements should be able to identify the nature of the ESR center.

Two papers appeared recently[16,17] reporting on ESR in x-ray-irradiated zirconia. The g values reported by the authors are almost the same as ours[9] but the line width is only half the one we found. The authors believe that the ESR center is a Zr^{3+} ion near an oxygen vacancy, while we think that the strong variation of $[C_{\mathrm{ESR}}]$ from crystal to crystal is an unequivocal proof that a foreign impurity is involved.

E_3 can be determined from the temperature dependence of $[C_{\mathrm{ESR}}]/n$. Equations (8) and (20) together with the explicit expressions for K_3 give

$$E_3 = \frac{\partial \ln[C_{\mathrm{ESR}}]}{\partial(1/kT)_{P(O_2)}} - \frac{\partial \ln n}{\partial(1/kT)_{P(O_2)}} \tag{23}$$

and it can be shown that the same equation holds at constant r. Here we have assumed that N_C does not depend on temperature and have also substituted $[F^{\mathrm{tot}}]$ for $[F^{(m-1)'}]$, since only a small minority of the foreign ions are reduced.

For crystals SA, SC, and SH, we get from Fig. 3 at $\log_{10} r = -2$

$$\log_{10}[C_{\mathrm{ESR}}]\ (\mathrm{cm}^{-3}) = (21 \pm 0.5) - 3365/T\ . \tag{24}$$

The concentration of electrons reported by Weppner[6] for the range 700–900 °C is at $\log_{10} r = -2$

$$\log_{10} n\ (\mathrm{cm}^{-3}) = 25.23 - 11\,450/T\ . \tag{25}$$

We therefore get from Eq. (23) that $E_3 = (\ln 10) \times 8085k = 1.60$ eV. Since $E_3 > E_1 > E_2$ in our model, this gives for E_1 and E_2 an upper limit of 1.60 eV.

From the equation

$$\log_{10}[F^{m'}] - \log_{10} n = \log_{10}\frac{[F^{\mathrm{tot}}]}{N_C} + \frac{E_3}{kT}\log_{10} e \tag{26}$$

which follows from Eq. (8) together with the explicit expression for K_3 we get that the ratio $[F^{\mathrm{tot}}]/N_C$ is given by the difference difference between the first terms on the right-hand side of Eqs. (24) and (25), and is $\cong 10^{-4.2}$. We know from the saturation value of $[C_{\mathrm{ESR}}]$ that $[F^{\mathrm{tot}}]$ is about 3×10^{19} cm^{-3}. The calculated value of N_C is therefore 5×10^{23} cm^{-3}. Since the effective number of states in the conduction band cannot be larger than the concentration of Zr ions which is 2.8×10^{22} cm^{-3} our calculated N_C is too high but it certainly points to a very narrow conduction band rather than a wide band in which $N_C \simeq 10^{19}$ cm^{-3}.

Our conclusion concerning a very narrow conduction band is reasonable both because of the low mobility of electrons and holes as reported by Weppner[6] and because a fit of his reported np product to a straight exponential temperature dependence or to the temperature dependence implied by his Eq. (17) gives $N_C = N_V = 2.8 \times 10^{22}$ cm^{-3}. Weppner's assumption of wide bands implicit in his Eq. (17) gives with $m_e = 1$ that $N_C = 8.4 \times 10^{19}$ cm^{-3} at 800 °C and is therefore not compatible with his experimental results. Also Park and Blumenthal in a recently published article[18] concluded, from measurements similar to those of Weppner, that electronic charge carriers in YSZ move by hopping and that N_C and N_V are not much smaller than the concentration of zirconium ions. An additional argument in favor of a narrow conduction band is given in the Appendix.

An essential difficulty here is that Weppner's values for n and p are based on measurements of partial electronic conductivity which give the product of concentration and mobility and of measurements which are variants of chemical diffusion. In such measurements one obtains, for example, for the electrons a diffusion constant which is the weighted average of all the electrons in the crystal. This has been pointed out some time ago by Heyne and Beekmans.[19] Since electrons reside not only in the conduction band but also in impurity and vacancy levels, the measured diffusion constant is much smaller than the true one for electrons in the conduction band and the concentration of electron calculated is correspondingly larger than the true one. Furthermore this effect is temperature dependent. Obviously this leads to wrong conclusions concerning the band structure, hence the value of E_3 calculated here is questionable. In order to work out the details of the band structure, one has to do additional measurements, such as time-of-flight measurements of mobility and attempt to derive the concentration of the defects from the deviation from stoichiometry (see below).

D. Signal dropoff at high oxygen pressures

As seen in Figs. 2(a) and 2(b) the ESR signal strength drops steeply at the right-hand end of most of the isotherms, in the vicinity of $\log_{10} r = 0$ which corresponds at 900 °C to $\log_{10} P(O_2) = -16.3$ atm. This drop should occur when the total number of available electrons, which is approximately $[F^{m'}]_{HT}$, is less than the number of empty acceptor sites including holes. In Fig. 6 we see that the intersection of $[F^{m'}]$ (which corresponds approximately to the measured concentrations in samples SD and SH) and p is near $\log_{10} P(O_2) = -11$ atm, the observed drop must therfore be caused by a second unknown impurity which has an empty or partially empty

energy level below that of the ESR centers and can thus trap the electrons located on these centers when the sample is cooled to room temperature. The concentration of this impurity is given by $[C_{\mathrm{ESR}}]$ at the dropoff, this is always less than 10^{18} cm^{-3}, corresponding to about 30 ppm.

The theoretical shape of the dropoff can be calculated from chemical equilibrium equations; it is shown in Fig. 2(b).

E. Identity of the center appearing at low $P(O_2)$

As mentioned the center responsible for the very dark color is not the same as the ESR center. After all levels related to impurity F are filled (saturation of ESR) additional levels causing the deep coloration begin to fill. We showed above that the ESR centers must be caused by impurities. We have no reason to suspect impurities for these additional levels, we shall therefore ascribe them to vacancies which have changed their valence state. Since a vacancy which has captured one electron should be ESR active (this is by definition an F center) and we find no such activity for the additional color centers we shall assume that we are dealing with V_{O}^{x} centers, i.e., vacancies which have captured two electrons. For this reason we have taken $E_1 > E_2$ in the parameters of Fig. 6.

F. Deviation from stoichiometry

It follows from Eq. (12) together with our conclusions above that

$$\Delta\epsilon \sim -\Delta(\mathrm{F}^{m'})/2 + \Delta V_{\mathrm{O}}^{x} \ . \tag{27}$$

This should be in principle detectable as a weight difference. For the values of Fig. 6 it is about 5×10^{-4} of the sample weight for a change from $\log_{10}P(O_2)=0$ to $\log_{10}P(O_2)=-35$ atm at 900 °C, this should be measurable.

ACKNOWLEDGMENTS

We wish to thank the CERES Corporation and Hrand Djevahirdjian S. A. for the donation of crystals, Dr. Y. Gernter for PIXE analysis and Dr. I. Laulicht for low-temperature measurements. This work was supported by the Fund for the Promotion of Research at the Technion.

APPENDIX

We get from Eq. (5) and some simple statistical mechanics that

$$\ln K_x = \tfrac{1}{2}\ln\left[\frac{2\pi m_{\mathrm{O}_2} kT}{h^2}\right]^{3/2} + \tfrac{1}{2}\ln\frac{kT^2}{\Theta_{\mathrm{rot}}} + \ln[\mathrm{O_O}] + \frac{\Delta\mu_{xO}}{kT} - \tfrac{1}{2} \tag{A1}$$

where m_{O2} is the mass of an oxygen molecule, Θ_{rot} its characteristic temperature of rotation ($2K$), and $\Delta\mu_{xO}$ the enthalpy change in reaction (1). We combine this with

$$\ln n = \ln N_C - \frac{E_1+E_2}{2kT} + \tfrac{1}{2}\ln(2K_x) - \tfrac{1}{2}\ln[Y'_{Zr}] - \tfrac{1}{4}\ln P(O_2) \tag{A2}$$

which follows from Eq. (13) and the explicit expressions for K_1 and K_2. We now assume that N_C does not depend on temperature, insert (A1) into (A2) and approximate the temperature dependence of n by $\ln n = A - B/T$. We then get that

$$\begin{aligned} A &= \ln n - \frac{1}{T}\frac{\partial \ln n}{\partial(1/T)} \\ &= \ln N_C + \tfrac{1}{2}\ln[\mathrm{O_O}] + \tfrac{3}{8}\ln\left[\frac{2\pi m_{\mathrm{O}_2} kT}{h^2}\right] \\ &\quad + \tfrac{1}{4}\ln\frac{kT^2}{\Theta_{\mathrm{rot}}} - \tfrac{1}{2}\ln[Y'_{\mathrm{Zr}}] - \tfrac{1}{4}\ln P(\mathrm{O_2}) - 0.78 \ . \end{aligned} \tag{A3}$$

Inserting numbers we get that at 800 °C and $P(O_2)=10^{-20}$ atm (10^{-15} Pa) $A - \ln N_C = 18.47$ in mks units. From Weppner's n values at $P(O_2)=10^{-20}$ atm we read that $A=84.29$ and get finally that $N_C = 3.8\times10^{28}$ m^{-3}. In a narrow-band approximation we should have $N_C = 2.8\times10^{28}$ m^{-3} (the concentration of zirconium sites), which agrees quite well with the calculated value. While the agreement could be fortuitous, this is another indication of the validity of the narrow-band model for stabilized zirconia.

[1] J. Genossar and D. S. Tannhauser, Cryst. Lattice Defects Amorph. Mater. **16**, 1 (1987).
[2] J. S. Thorp, A. Aypar, and J. S. Ross, J. Mater. Sci. **7**, 729 (1972).
[3] K. K. Ermakovich, V. N. Lazukin, V. M. Tatarintsev, and I. V. Chepeleva, Fiz. Tverd. Tela (Leningrad) **19**, 3488 (1977) [Sov. Phys. Solid State **19**, 2040 (1977)].
[4] J. Genossar and D. S. Tannhauser, J. S. S. Ionics **28–30**, 503 (1988).
[5] H. Schmalzried, Z. Elektrochem. **66**, 572 (1972).
[6] W. Weppner, Z. Naturforsch. **31a**, 1336 (1976).
[7] K. D. Becker and D.S. Tannhauser (unpublished).
[8] R. Ben-Michael and D. S. Tannhauser (unpublished).
[9] J. Shinar, D. S. Tannhauser, and B. L. Silver, Solid State Commun. **56**, 221 (1985).
[10] D. A. Wright, J. S. Thorp, A. Aypar, and H. P. Buckley, J. Mater. Sci. **8**, 876 (1973).
[11] V. R. PaiVerneker, A. N. Petelin, F. J. Crowne, and D. C. Nagle, Phys. Rev. B **40**, 8555 (1989).
[12] D. L. Dexter, Phys. Rev. **101**, 48 (1956).
[13] R. H. Silsbee, Phys. Rev. **103**, 1637 (1956).
[14] H. W. den Hartog, doctoral thesis, Groningen University, 1969.

1969.
[15]K. K. Ermakovich, V. N. Lazukin, I. V. Chepeleva, and V. I. Aleksandrov, Fiz. Tverd. Tela (Leningrad) **18**, 1755 (1976) [Sov. Phys. Solid State **18**, 1022 (1976)].
[16]C. B. Azzoni and A. Paleari, Phys. Rev. B **40**, 6518 (1989).
[17]C. B. Azzoni and A. Paleari, Phys. Rev. B **40**, 9333 (1989).
[18]J.-H. Park and R. N. Blumenthal, J. Electrochem. Soc. **136**, 2867 (1989).
[19]L. Heyne and N. M. Beekmans, Proc. British Ceramic Soc. **19**, 229 (1971).